IEEE Access
Multidisciplinary ⋮ Rapid Review ⋮ Open Access Journal

Received March 21, 2021, accepted April 11, 2021, date of publication April 15, 2021, date of current version April 27, 2021.

Digital Object Identifier 10.1109/ACCESS.2021.3073490

Application of Computer Method in Solving Complex Engineering Technical Problems

YUE WU[1,2], WEIGUO QIAO[1,2], YANZHI LI[1,2], YABING JIAO[3], SHUAI ZHANG[1,2], ZONGHAO ZHANG[4], AND HUINI LIU[1,2]

[1]Shandong Key Laboratory of Civil Engineering Disaster Prevention and Mitigation, Shandong University of Science and Technology, Qingdao 266590, China
[2]College of Civil Engineering and Architecture, Shandong University of Science and Technology, Qingdao 266590, China
[3]Dongying Survey and Surveying Institute, Dongying 257091, China
[4]Laoshan District Urban Administration Bureau, Qingdao 266061, China

Corresponding author: Weiguo Qiao (qiaowg1@163.com)

This work was supported by the National Natural Science Foundation of China under Grant 51774192 and Grant 51704183.

ABSTRACT In order to verify the applicability of the computer numerical simulation method under complex engineering conditions, and solve the problem that it is difficult to guarantee the normal construction of underground projects with a depth of more than 1 km (it is difficult to carry out multiple field attempts under high-depth conditions, and if you simply use ordinary the calculation method, its calculation accuracy is difficult to guarantee). For the construction of complex geological conditions of an underground mine with a depth of 1300 m in the Central Plains of China, based on the finite difference method (FDM) with high calculation accuracy, using FLAC^{3D} software based on FDM, and using progressive design method (PDM), design a variety of different schemes and analyze the mechanism of force and deformation of the surrounding rock mass of the project. Apply the obtained optimal scheme in actual engineering, and monitor the actual force and deformation. Comparing the results of the computer numerical simulation with the monitoring results, the results show that the computer numerical simulation method can also have good application in the actual engineering under the geological conditions of ultra-kilometer depth. It also provides theoretical basis and technical guidance for engineering hypothesis under approximate conditions.

INDEX TERMS Computer numerical simulation method, FDM, FlAC^{3D}, PDM, support schemes, field monitoring.

I. INTRODUCTION

Computer numerical simulation methods have penetrated into all walks of life and are widely used in various fields. MOHAMED [1] Aiming at an obstacle guidance path refinement algorithm that uses obstacles in the environment to quickly plan collision-free paths, OGPR∗ is proposed, using computer numerical simulation methods, compared with the most advanced algorithms in the literature, The proposed algorithm has remarkable performance. TAK [2] through three-dimensional finite element analysis, proposed an analysis method and algorithm considering the nonlinear effects of magnetic saturation and slotting, and verified the effectiveness of the proposed analysis and design method and the axial flux permanent magnet motor Sex. KANEKO[3] based on the existing Japanese distribution network as a model and used it for computer numerical simulation, proposed a method to determine the optimal radial loop configuration in the photovoltaic distribution network, and evaluated the effectiveness of the configuration, The result has good reliability. TIAN [4] In order to study the machinability of coal ploughs, improve the performance of coal ploughs, so as to achieve efficient mining of coal mines. A three-dimensional model was established by computer numerical simulation. The results show that the maximum error of the force obtained by simulation and experiment is 7.849 and the difference is 6.5%. Combining the discrete element method with the finite element method improves the performance of the plowshare. The simulation results are verified through experiments and industrial production, which proves the accuracy and feasibility of using DEM to study the cutting performance of the coal plough.

LEI [5] through the inversion analysis of the ground penetrating radar echo signal, it is found that the traditional forward model adopts the ladder approximation method to produce certain errors. Then, an accurate and efficient

The associate editor coordinating the review of this manuscript and approving it for publication was Guido Lombardi.

numerical model of the underground pipeline ground penetrating radar forward model was established by using computer numerical simulation methods, and it was proved that the method can effectively cut off the computational domain of Sin Euler. Through the simulation research of different underground pipeline models, the GPR image characteristics of metal pipes, plastic pipes and concrete pipes filled with air and water are obtained. Numerical simulation results show that the parallel-conformal Singular Euler algorithm effectively reduces the pseudo-diffraction wave caused by the step approximation, and improves the calculation efficiency of the model in metal and non-metal media. JAVAD [6] uses computer numerical simulation technology, Monte Carlo method, combined with approximate linear model for mathematical modeling while considering the uncertainty of electricity prices and distribution network load. The simulation results show that the model has the required efficiency, reduces the load on the large-capacity feeder, and delays the construction of the new feeder. It has also been observed that rearranging the distribution grid can reduce grid losses. In addition, with the help of rescheduling, the number of interrupted loads can be significantly reduced. MIKKO [7] proposed a comprehensive workflow development data-driven agent model, including data generation based on physical simulation and experimental design, training data preprocessing, training and testing agents. Comparing neural networks and gradients to improve the accuracy and computational efficiency of surrogacy by choosing experimental design methods for decision tree modeling and simulation of the behavior of the torque permanent magnet synchronous machine. The results show that the use of domain knowledge to create agent models can improve agent accuracy. The actual result is also close to the finite element simulation result.

Although computer numerical simulation methods have been widely used in all walks of life, in recent years, due to the inability of human beings to fully go deep underground for actual operations, their applications in underground engineering have become more and more Wu [8], [9]. In the underground coal mine construction project, many scholars have explored in many aspects. Du [10] In order to study the influence of the number of cables on the simulation results when the length of the anchor rod is the same, the cable structural unit in FLAC^{3D} is used to establish the anchor rod model, and the influence of the number of cables and the stiffness of the anchoring agent on the results is studied through the drawing simulation test. The results show the good application rules of bolts under different conditions. Zhang [11] used theoretical analysis, field test and numerical simulation to propose an integrated support technology of shotcrete, anchor and penetration. The research results have realized effective control of roadway deformation and can provide reference for other similar areas in the mine. Lu [12]. Combined with the results of numerical simulation analysis, the existing roadway filling and sidewall backfilling, floor reinforcement, and reinforcement of the existing roadway at a location of 300m underground are proposed, and the support is strengthened for the locations where stress concentration is easy to occur, so as to ensure the safety and reliability of the stope. Zhang [13] Aimed at the difficulty of controlling the stability of the mining roadway under the condition of repeated mining in steep coal seams, he proposed the support principle of ''active support, strengthened control of key parts'', using ''strong bolt and long anchor cable and W steel belt'' The ''reinforced mesh'' asymmetrical coupling support method effectively controls the deformation and destruction of the roadway. The research results can provide a reference for solving the difficult problem of steeply inclined coal seam roadway support. Wu [14] Taking the 1102 track coal roadway in Qiuji coal mine as the background, by constructing a hard roof deformation analysis model, quantifying the role of five ash thickness in controlling the roadway deformation, using numerical simulation to verify the theoretical calculation results, and passing field tests and monitoring complex Empirical research results. The method used in combination with the obtained results can effectively meet the safety production requirements. He [15] Aiming at the problem of supporting structure at the bottom of the scope of soft fractured rock masses, FLAC^{3D} numerical simulation was used to analyze the advantages and disadvantages of the three existing support methods in the mine, and the displacement and stress simulation analysis was used to analyze the excavation and support process of the horizontal roadway. And the stability of the approach, the results verify the safety and stability of the project in this area. Qin [16] conducted research on the failure mechanism of roadway instability and support and reinforcement schemes in deep broken and weatherable rock masses, and put forward the deficiencies of the existing support schemes. Through theoretical analysis, they obtained roadway stability control strategies and solutions suitable for such conditions. Supporting structure parameters, using numerical analysis to study the surrounding rock displacement and stress evolution law before and after roadway support in broken rock mass, verifying the rationality of the optimized support plan. The results show that the numerical calculation results can ensure the stability of the surrounding rock during tunneling and mining, control the deformation and stress within a reasonable range, and meet the mine safety and normal production requirements.

In the above research on engineering technical issues, although good results have been achieved, the buried depths are all below one thousand meters, and there is a lack of research on technical issues such as engineering construction above one thousand meters. The increase in depth makes the geological situation more and more complicated. Many actual engineering cases and studies by scholars have shown that it is not only difficult to make multiple field trials under high-depth conditions, but also if ordinary calculation methods are simply used, once the underground depth is increased, the calculation accuracy cannot be guaranteed. In order to solve these problems, this paper deals with the complex geological conditions engineering construction problem of an underground mine with a depth of 1300 m in the Central Plains of

TABLE 1. Geologic description.

No.	Rock types	Depth (m)	Thickness (m)
1	Sandy mudstone	1334.46	12.2
2	Siltstone	1337.02	2.55
3	Sandy mudstone	1341.14	4.15
4	Argillaceous siltstone	1343.55	2.43
5	Coarse grained sandstone	1352.73	9.16

TABLE 2. Mine water inflow.

Depth (m)	Thickness (m)	Water inflow (m^3/h)
208.73	5.54	4.53
229.35	12.02	5.92
477.16	9.24	6.76
509.87	3.69	1.98

China, based on the finite difference method (FDM) with high calculation accuracy, using FLAC^{3D} software based on FDM, and using progressive design method (PDM), design a variety of different schemes and analyze the mechanism of force and deformation of the surrounding rock mass of the project. Apply the obtained optimal scheme in actual engineering, and monitor the actual force and deformation. The computer numerical simulation results are compared with the monitoring results, and the results are in good agreement. The method in this paper not only solves the problem that it is difficult to guarantee the normal construction of the underground engineering with a depth of more than one kilometer, but also ensures the calculation accuracy and reliability. The obtained scheme can be used for reference by other projects and has great practical engineering significance.

II. ENGINEERING OVERVIEW

Based on the results of geological exploration, a brief description of the geological and hydrological conditions of the area is given.

A. GEOLOGICAL CONDITION

The geological conditions near the mine are shown in Table 1.

Lithology description:

(a) Sandy mudstone: mainly gray, thin-layered, argillaceous structure, uneven sandy, compact, brittle, inclined bedding, and flat fracture.

(b) Siltstone: gray, gray-green, thin-layered, silt-like structure, with small upper particles, uneven argillaceous cementation, thin-layered locally, dense, and flat fractures.

(c) Argillaceous siltstone: gray, gray-green, thin-layered, silt-like structure, with small upper particles, uneven argillaceous cementation, thin layered locally, dense, and flat fracture.

(d) Coarse grained sandstone: gray-white, light gray-green, thick layered, coarse-grained sand-like structure, the upper part is relatively coarse, with cracks, argillaceous cement, oblique bedding, and flat fracture.

B. HYDROLOGY OVERVIEW

The water inflow of the mine shaft is shown in Table 2.

It can be seen from table 2 that the hydrogeological conditions of the mine are relatively complex, and the discharge of mine water inflow should be well handled in the construction process.

III. NUMERICAL SIMULATION ANALYSIS OF INITIAL SUPPORT SCHEME AND BRIEF DESCRIPTION OF FAILURE MECHANISM

The finite difference method (FDM) is a numerical calculation method based on the difference principle. It uses the difference quotient of the function at each discrete point to approximate the partial derivative of the point, and converts the boundary value problem to be solved into a set of corresponding difference equations. Then, the function value of the difference equations (linear algebraic equations) at each discrete point is solved to obtain the numerical solution of the boundary value problem.

The finite difference method has many ideas and methods, such as conservative difference format, time correlation method, step-by-step method, etc. Take the step-by-step method as an example for a brief introduction.

Decompose each time step of a complex problem into several intermediate steps, such as decomposing a multi-dimensional problem into several one-dimensional problems according to coordinates, and then use the difference method to solve these relatively simple intermediate steps, and finally get an approximate solution to the original problem, this kind of method is called step-by-step method. Alternating direction method, estimation-correction method, time division method, factorization method, etc. fall into this category. Solve the problem with a two-dimensional parabolic equation:

$$\frac{\partial u}{\partial t} = \frac{\partial^2 u}{\partial x^2} + \frac{\partial^2 u}{\partial y^2} \tag{1}$$

$$u|_{i=0} = f(x, y), \quad (x, y \in D) \tag{2}$$

$$u = 0, \quad (x, y \in D) \tag{3}$$

As an example, using an explicit format to solve, the time step is subject to stability conditions:

$$\Delta t \leq \frac{1}{2\left(\frac{1}{\Delta x^2} + \frac{1}{\Delta y^2}\right)} \tag{4}$$

The limitation of using the implicit format boils down to large linear algebraic equations, which is more troublesome to solve. In 1955, Peisman-Rashford proposed the alternate direction implicit format:

$$\frac{u_{ij}^{n+1}-u_{ij}^{n}}{\Delta t}=\frac{1}{\Delta x^2}\delta_x^2 u_{ij}^{n+1}+\frac{1}{\Delta y^2}\delta_y^2 u_{ij}^{n},\quad (fisrt-step) \tag{5}$$

$$\frac{u_{ij}^{n+2}-u_{ij}^{n+1}}{\Delta t}=\frac{1}{\Delta x^2}\delta_x u_{ij}^{n+1}+\frac{1}{\Delta y^2}\delta_y u_{ij}^{n+2},\quad (second-step) \tag{6}$$

($i = 1, 2,\ldots, \text{N-1}; j = 1, 2,\ldots, \text{M-1}; n = 0, 1, 2,...$)

For the central difference operator, the first step is implicit in the x direction and explicit in the y direction. The second step is the opposite. Two-step synthesis of unconditionally stable format. Since each step can be solved by the chasing method, the understanding method is greatly simplified. After the emergence of the alternating direction method, various forms of step-by-step formats have been further developed, and can be extended to any dimensional equation or system of equations.

The finite difference method has become the main numerical method for solving various mathematical and physical problems, and it is also one of the main numerical methods in computational mechanics. Some methods of solving partial differential problems (such as characteristic line method, straight line method) are essentially a form of difference method.

And FLAC3D is a kind of numerical simulation software that makes full use of FDM for calculation.FLAC3D is an extension of the two-dimensional finite difference program FLAC2D, which can simulate the mechanical characteristics and plastic flow analysis of three-dimensional structures of soil, rock and other materials. FLAC3D uses the finite difference method (FDM), the actual structure is fitted by adjusting the polyhedron elements in the three-dimensional mesh. The constitutive model of the element material can be linear or nonlinear [17], [18].

Under the action of external force, when the material yield flow, the mesh will undergo corresponding deformation and movement (large deformation mode). Using explicit Lagrange algorithm and hybrid discrete partition technology, FLAC3D can simulate the deformation and failure of materials very accurately [19], [20].

Nowadays, most of the deep well large section roadways in China have complex geological environment and poor supporting conditions. Whether it can ensure the stability of the surrounding rock and the safe use of the roadway, the rigidity and strength of the initial support system are particularly important. Therefore, this chapter takes a mine roadway in the Central Plains area as the engineering background, uses FLAC^{3D} numerical simulation and other methods to analyze and discuss the stress and deformation under the initial support scheme of the large-section roadway in deep mines, and briefly describe the causes of damage. The design section of the coal mine roadway is 8.2 × 6.6 m, and it adopts the semicircular arch section.

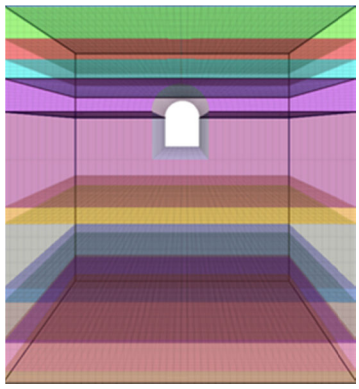

FIGURE 1. Model drawing of roadway and surrounding rock.

A. ESTABLISHMENT OF THE NUMERICAL MODEL

In order to show the effect of the numerical model of the support scheme more intuitively, the force and deformation of the roadway section is simulated and analyzed. The numerical calculation model is shown in Figure 1. The strata from top to bottom are sandy mudstone, argillaceous siltstone, argillaceous siltstone, sandy mudstone, sandy mudstone, sandy mudstone, coarse-grained sandstone, sandy mudstone, sandy mudstone, coarse-grained sandstone, and sandy mudstone.

In order to eliminate the size effect, the model size is about 5 times the actual size of the roadway. The specific size is 45 m wide, 50 m high, and 50 m long. The Mohr-Coulomb calculation model is used and divided into 62489 cells. The side of this model restricts horizontal movement and the lower surface Fixed. By calculating the weight of the overlying rock mass, a load of 25.4 MPa is applied to the upper surface to simulate the upper load boundary. The thickness and mechanical parameters of the rock layer are selected according to actual engineering conditions. The surrounding rock of the roadway uses solid elements for simulation calculation, and the bolt and anchor cable use cable structure for simulation calculation. The steel mesh is considered in accordance with the principle of equivalence, that is, the elastic modulus of the steel arch and the steel mesh is converted into the concrete spray layer, and the elastic modulus E of the concrete spray layer is equivalently considered.

The mechanical parameters of the surrounding rock input in the numerical calculation should be the mechanical parameters of the natural rock mass, and the value of the mechanical parameters plays a key role in the accuracy of the numerical simulation calculation results. The engineering geological lithology of this project case is siltstone, sandy mudstone, argillaceous siltstone and coarse grained sandstone. According to field investigations, mechanical parameter tests and geological exploration reports, combined with the rock mass quality classification system to determine the quality level of the rock mass, physical and mechanical parameters such

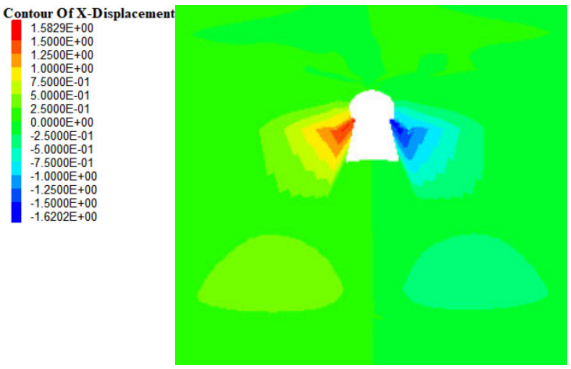

(a) Horizontal displacement distribution of roadway excavation without support

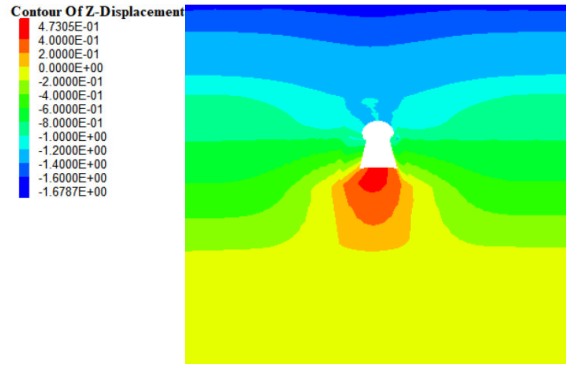

(a) Vertical displacement distribution of roadway excavation without support

FIGURE 2. Unsupported displacement cloud image of roadway excavation.

as the uniaxial compressive strength of the rock mass are obtained from indoor rock physical mechanics experiments.

The elastic modulus of the anchor rod used is 2.0×10^5 MPa, and the prestress is 5t. The elastic modulus of the anchor cable is 1.95×10^5 MPa, Ø22, the row spacing is 1400 mm, and the prestress is 15t. The elastic modulus of shotcrete is 2.56×10^4 MPa, Poisson's ratio is 0.21, thickness is 150 mm, and strength grade is C_{20}. Table 3 shows the physical and mechanical parameters of the surrounding rock and supporting structure used in this simulation. In this simulation calculation, the surrounding rock of the roadway is regarded as an isotropic homogeneous body, and the influence of groundwater on the deformation of the surrounding rock is not considered.

B. STRESS AND DEFORMATION ANALYSIS OF ROADWAY WITHOUT SUPPORT AFTER EXCAVATION

After the excavation of the roadway without support, numerical simulation calculation is performed, and the roadway deformation is shown in Figure 2.

It can be seen from Figure 2 that after the roadway is excavated, the stress of the surrounding rock mass is redistributed, and most of the lateral displacement is concentrated on the straight walls on both sides of the roadway and the shoulder between the straight wall and the vault. The maximum deformation of the right side and the right side reaches 1583 mm and 1627 mm, indicating that the stress in this part of the area is relatively concentrated; both the dome and the bottom plate are deformed to a large extent, the maximum displacement at the dome is 1291 mm, and the maximum displacement at the bottom plate is 473 mm. Therefore, if the initial support treatment is not carried out in time after the excavation of the roadway, it will soon be subjected to the pressure of the surrounding rock and produce large deformation, so that the roadway will collapse and damage.

C. INITIAL SUPPORT SCHEME DESIGN

The initial support form is bolt mesh shotcrete support, and the specific design parameters are as follows.

Bolt: high-strength pre-stressed bolt is adopted, and the parameters of the bolt are as follows: the spacing between the rows is anchored by a coiled resin cartridge, and the bolt tray is provided. High-strength prestressed resin bolt, specification Ø22 × 2400 mm, row spacing 800 × 800 mm, anchored by 2 resin anchoring agents, designed anchoring force 150 t, pre-stress 5 t.

Metal mesh: use steel bars with a diameter of 6.5 mm, lapped and processed into a grid 100 × 100 mm sheet structure, and the lap length between the grids is 100 mm.

Concrete: Use C_{20} shotcrete with a thickness of 150 mm.

After the primary support was used for 28-29 days, the secondary support of reinforced concrete masonry with strength C_{40} and thickness of 400 mm was used.

D. DEFORMATION AND FAILURE CHARACTERISTICS AND INFLUENCING FACTORS OF ROADWAY UNDER INITIAL SUPPORT SCHEME

1) DEFORMATION AND FAILURE CHARACTERISTICS OF ROADWAY

a: THE BOTTOM HEAVE PHENOMENON IS SERIOUS

With the continuous increase of the mining depth of the mine, the large-section roadway in the deep shaft will produce serious bottom heave phenomenon (that is, the large deformation of the floor of the surrounding rock of the roadway). Floor heave phenomenon is the deformation and failure form of the surrounding rock of the roadway along the vertical direction [21]. Floor deformation is the most likely to occur in the surrounding rock of the roadway. Most roadways have serious floor heave phenomenon as the buried depth increases, and the treatment of floor heave has also become a problem. One of the difficult problems of deep mine roadway support.

The tunnel section of the mine adopts a semicircular arch section. Due to the deep burial, the surrounding rock is relatively broken. According to the previous field data monitoring report, within two months after the construction, the bottom heave appeared obvious, and the heave amount reached 500 mm, and the heave type was stress-type heave. As shown in Figure 3, the current roadway can no longer meet the

TABLE 3. Mechanical parameters of surrounding rock.

Rock types	Strata thickness (t/m)	Average rock density (ρ/g·cm^{-3})	Elasticity modulus (E/MPa)	Poisson ratio (μ)	Cohesion (c/MPa)	Friction angle (φ/°)	Tensile strength ($Tens$/MPa)
Sandy mudstone	12.2	2.31	2.81×104	0.20	1.82	26	2.25
Siltstone	2.55	2.40	2.39×104	0.14	6.72	43	2.41
Sandy mudstone	4.15	2.15	2.79×104	0.22	1.79	27	2.26
Argillaceous siltstone	2.43	2.19	2.92×104	0.28	4.15	53	1.40
Coarse grained sandstone	9.16	2.48	4.86×104	0.13	8.42	51	3.19

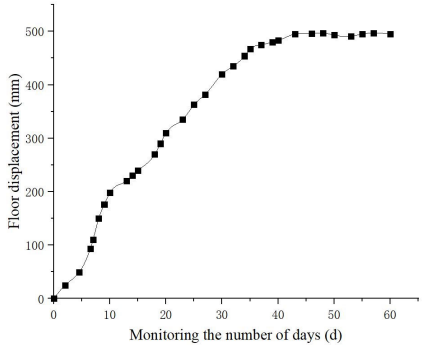

FIGURE 3. Bottom heave monitoring curve.

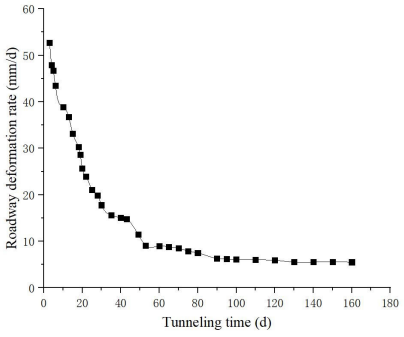

FIGURE 4. Relationship curve between roadway deformation rate and tunneling time.

requirements of safety and production use, and it needs to be repaired and reinforced.

b: BRITTLE TO EXTENDED TRANSFORMATION CHARACTERISTICS

The stress level of shallow buried projects is relatively low, and the surrounding rock is mostly brittle failure [22]. As the mining depth increases, the roadway changes from a low stress level to a high stress level, and the brittle failure of part of the rock changes to ductile failure. The tunnel depth of this coal mine is more than 1300 m, the surrounding rock strength of the tunnel is low, and most of the rocks exhibit ductile failure in a high in-situ stress environment. Therefore, the brittle-ductile transformation characteristic of rock mass is one of the characteristics of deformation and failure of mine tunnels.

c: LAGE DEFORMATION AND STRONG RHEOLOGICAL PROPERTIES

According to the previous field data monitoring report, due to its high ground stress characteristics, the deep mine roadway will produce considerable elastic-plastic properties, and the internal deformation energy of the surrounding rock can be released after the roadway is excavated. Therefore, at the beginning of excavation, the roadway will show a great deformation rate, and the deformation has a time effect that changes with the change of the driving time [23], as shown in Figure 4.

2) BRIEF INTRODUCTION OF INFLUENCING FACTORS OF SURROUNDING ROCK DEFORMATION AND FAILURE

a: THE ROCK MASS IS CRACKED AND THE ROCK STRENGTH IS LOW

The lithology of the surrounding rock is one of the important factors that affect the construction of the mine and the selection of the support plan for the shaft and roadway [24]. In order to select the roadway support plan reasonably, it is necessary to select rock samples at representative locations at the beginning of the roadway excavation. Through physical and mechanical properties experiments on rock samples, it is found that the integrity of the rock mass is general, the rock is broken, the rock quality index (RQD) of the surrounding rock is not high, the continuity of the surrounding rock of each layer is poor, and the integrity of the surrounding rock is not well, this causes its carrying capacity to be low. X-ray diffractometer was used to analyze the phase composition of the rock samples, and the results of the spectrum analysis of

TABLE 4. Test result of mineral composition of surrounding rock of roadway.

Sample position		No.	Mineral content (%)			
			Quartz	Pearl clay	Kaolinite	Anorthite
Opening of horizontal roadway section	Roof	1	38.5		21.2	35.9
	On the left roadway baseline	2	47.2		20.7	31.7
	Under the left roadway baseline	3	51.7		17.6	27.2
	On the right roadway baseline	4	39.6		14.9	35.6
	Under the right roadway baseline	5	49.8		18.3	33.7
	Floor	6	51.2	4.9	25.1	26.8

the mineral composition in the surrounding rock are shown in Table 4.

The rock mineral composition analysis test shows that the main composition of the rock in the surrounding rock of the newly built roadway is quartz, kaolinite, anorthite and a very small amount of nacre. The average value is about 46.33% for quartz and 19.63% for kaolinite. Anorthite accounted for 31.82% and pearl clay accounted for 0.82%. That is, the surrounding rocks of mine tunnels are mainly quartz, kaolinite, and anorthite. Although kaolinite is a weakly swelling clay mineral, it is easy to muddy, hydrolyze and soften when exposed to water. If it encounters water or other high ground stress, its rheology is also very strong [25]. In addition, the strength of the rock itself and the structural characteristics of the surrounding rock also have a decisive influence on the deformation and failure of the surrounding rock of the roadway. There are many mechanical indicators reflecting the strength of rocks, among which the uniaxial compressive strength of rocks is representative and relatively easy to obtain [26]. The more common influences of surrounding rock structure are bedding and joints.

b: IMPACT OF BURIED DEPTH

The mine roadway is affected by nearby rock faults, coupled with its high in-situ stress characteristics, the surrounding rock deformation presents brittle-ductile transition characteristics, and the bearing capacity of the rock mass is reduced. Therefore, when the supporting body is damaged, the deformation of the roadway increases sharply, which causes great difficulties for the support of the large-section roadway. A lot of practice and research data show that the gravity of most roadway engineering support systems is proportional to the bulk density and buried depth of the overlying rock, that is, $P = \gamma H$ [24]. As the buried depth of the project increases, the ground stress becomes larger, and the rheology or swelling of shale, mudstone and other rocks with low cementation strength is very obvious under the influence of the increased buried depth. The underground engineering of mine tunnels is more than 1300m deep. If the mine tunnels are to be deformed and damaged, they are inseparable from the gravity influence of the overlying rock layer [27]–[29].

c: INFLUENCE OF GROUNDWATER

The compressive strength and elastic modulus of the rock will be reduced by the influence of groundwater. The greater the reaction strength, the greater the influence of hydration on the fracture mechanics index. The internal cohesive force of the surrounding rock of the roadway is greatly reduced under the action of the osmotic pressure of up to 7MPa in the deep mine roadway, and the properties of the rock mass also change accordingly. [30], [31].

By analyzing the mineral composition of the rock samples at representative locations around the mine tunnel, it is found that, except for quartz, the other components are affected by water to some extent. Mainly manifested as swelling, softening and disintegration in water. In addition, the acidity and alkalinity of groundwater is weakly alkaline, and it is also corrosive to rock-forming minerals.

d: THE IMPACT OF GROUND TEMPERATURE CHANGES

As the burial depth increases, the temperature of the surrounding rock is increasing. The temperature measurement results show that the deeper the ground, the higher the ground temperature. The temperature gradient generally ranges from 30 to 50 °C/km, and the temperature gradient under normal conditions is 3 °C/100 m [32]. In some areas, such as near faults or abnormal local areas with high thermal conductivity, the geothermal gradient is sometimes as high as 200 °C/km. The mechanics and deformation properties of rock masses under conditions beyond normal temperature

are quite different from those under ordinary environmental conditions. The ground temperature can cause the rock mass to expand and contract with heat, and a 1 °C change in the temperature of the rock mass can produce a ground stress change of 0.4 to 0.5 MPa. The in-situ stress changes caused by the increase in rock mass temperature will have a significant impact on the mechanical properties of the engineering rock mass.

Before and after the excavation of the roadway, the temperature field near the surrounding rock of the roadway changes, forming a temperature gradient between the surface of the roadway and the surrounding rock in the depth, generating temperature stress, and acting on the supporting structure or the surrounding rock mass of the roadway, causing separation of the surrounding rock of the roadway, which has extremely adverse effects on the stability of the surrounding rock of the roadway. The temperature in the mine tunnel reaches about 36°C, which is one of the factors affecting the deformation and failure of the surrounding rock [33].

e: UNREASONABLE SUPPORTING STRUCTURE

During the excavation of deep wells and large cross-section roadways, the structure bottom is slow and the bottom of the structure remains open for a long time. However, only when a closed ring structure is formed can the structure remain stable [34]. In addition, improper selection of materials for the support structure will also make it difficult to meet the stability requirements of the surrounding rock of the roadway.

f: CONSTRUCTION FACTORS

The construction technology, method and support timing are all important factors to ensure the stability of the surrounding rock of a large section roadway in a deep mine. The roadway uses the blasting method to excavate the roadway, and the vibration caused by the blasting will affect the stability of the surrounding rock. The reasonable choice of support timing is also very important. Premature support will reduce the overall stability of the support structure. If the support is too late, the excessive deformation of the surrounding rock of the roadway will increase the force of the support structure, and eventually there will be risks of damages such as topping and gangling.

IV. NUMERICAL SIMULATION ANALYSIS OF THREE OPTIMIZED ROADWAY SUPPORT SCHEME

A. PROPOSAL OF THREE OPTIMIZED ROADWAY SUPPORT SCHEME

Advanced design method (PDM): because the design scheme needs to consider the cost, reasonable use of resources and other factors, but the actual effect of the scheme is unknown, it is necessary to gradually optimize the known traditional scheme and analyze its feasibility to find the best answer [8].

The incremental design method is mainly an optimization idea, which needs to be analyzed in detail based on the actual situation. Based on this idea, Ni [35] researched and improved the progressive structural optimization method, and applied the improved method to specific engineering examples. best plan. Wang [36] based on this optimization method, combined with the powerful feature extraction capabilities of Convolutional Neural Networks (CNN), used for parameter optimization of the divide and conquer algorithm. Under the comparative analysis of multiple schemes, the calculation results were converged to a more optimized state, and the finally obtained scheme achieved better results in practical applications. It can be seen that the idea of progressive design method is widely used and has good application in engineering practice.

TABLE 5. Supporting scheme design table.

Support scheme	Length of bolts (m)	Row spacing between bolts (mm)	Length of bottom bolts (m)	Anchor cable length (m)
Scheme 1	2.2	800	2.4	-
Scheme 2	2.2	800	2.4	7.6
Scheme 3	2.4	700	2.6	9.6

It can be seen from the foregoing that after excavation, the top of the roadway arch was initially supported by bolting with mesh and shotcrete. The supporting effect was not ideal, and the deformation of the bottom plate and the two sides was still serious, which could not meet the normal use of the roadway. When optimizing the support scheme, based on the previous analysis of the results of the geological profile and the causes and characteristics of the damage, referring to the common support methods, combined with the mine construction specifications (GBT35056-2018 and other industry norms), three new support plans were designed using PDM. All three support schemes adopt full-face support.

Supporting scheme 1: bolts, shotcrete, grouting and hang metal mesh.

Support scheme 2: bolts, metal mesh, anchor cables, shotcrete and grouting.

Supporting scheme 3: bolts, metal mesh, anchor cables, shotcrete and grouting.

The grouting bolts used in the three schemes are all arranged in a plum blossom shape with the resin bolts spaced apart and the diameter of the bolts is 20 mm. The shotcrete strength grade is C_{20}, the thickness is 150 mm, the bottom angle anchor diameter is 22 mm, and the included angle is 30°. The diameter of the three anchor cables is 21.8 mm, and the cross-sections are arranged with 9 cables, and the spacing between rows is 1400 mm.

FLAC^{3D} is a finite difference software using finite difference method. Three different schemes of PDM design are analyzed by FLAC^{3D} software, which is the combination of FDM and PDM. For make the three supporting schemes more intuitively reflected in the numerical simulation, the

numerical simulation model diagrams of the three supporting schemes are now presented.

B. DISPLACEMENT ANALYSIS OF ROADWAY SURROUNDING ROCK

1) VERTICAL DISPLACEMENT

The displacement of the surrounding rock of the roadway is the most intuitive and accurate manifestation of the force of the surrounding rock. In order to deeply analyze the supporting effect of each supporting scheme, it is necessary to analyze the vertical displacement and horizontal displacement of the surrounding rock of the roadway. The different vertical displacement distribution diagrams of the three schemes are shown in Figure 6.

Figure 6 shows the vertical displacement cloud diagrams under different support schemes. The vertical displacement of the surrounding rock of the roadway appears in the form of an arch. For the roof deformation, the maximum value of the roof sink in scheme 1 is 74.5 mm, the stability of the roof is poor, and there is still a serious separation phenomenon on the roof, which may cause the risk of falling. Compared with the scheme 1, the maximum deformation of the roof of the second scheme is reduced from 74.5 mm to 55.6 mm. It can be seen that the scheme 2 has achieved a good supporting effect. The maximum deformation of the roof in scheme 3 is 51.7 mm, the surrounding rock of the roof is relatively stable, and its supporting effect is improved compared with scheme 2.

From the perspective of the deformation of the floor, the plan has the worst protection effect. The maximum deformation of the floor is as high as 101.9 mm, and the surrounding rock at the floor has undergone severe deformation. In scheme 2, the maximum deformation of the floor is 82.7 mm, which can effectively restrain the deformation of the surrounding rock. Due to the addition of anchor cables in the supporting process of scheme 2, the stress on the surrounding rock on the surface of the roadway is transferred from the shallow part to the deep part, thereby restraining the excessive deformation of the floor. The maximum deformation of the floor of the scheme 3 is 71.8 mm. At this time, the stability of the surrounding rock of the roadway is better, which can ensure the normal use of the roadway to a large extent, and the surrounding rock can maintain high stability.

2) HORIZONTAL DISPLACEMENT

For the displacement and deformation of the two sides, the maximum deformation of the left and right sides of the scheme 1 is 72.6 mm and 71.3 mm respectively. The surrounding rock of the gang has poor stability, and there is a risk of spalling. The maximum deformation of the left and right sides of the roadway in the scheme 2 is 59.9 mm and 58.9 mm, respectively. Compared with the scheme 1, the deformation is significantly reduced, and the stability of the surrounding rock at the side is improved. The maximum deformation of the left side of the roadway in scheme 3 is 57 mm, and the maximum deformation of the right side is 55.8 mm, which has improved the supporting effect compared to scheme 2. Generally speaking, the deformation of the surrounding rock shows a distribution law of ''the deformation of the left side is greater than that of the right side on the roadway''.

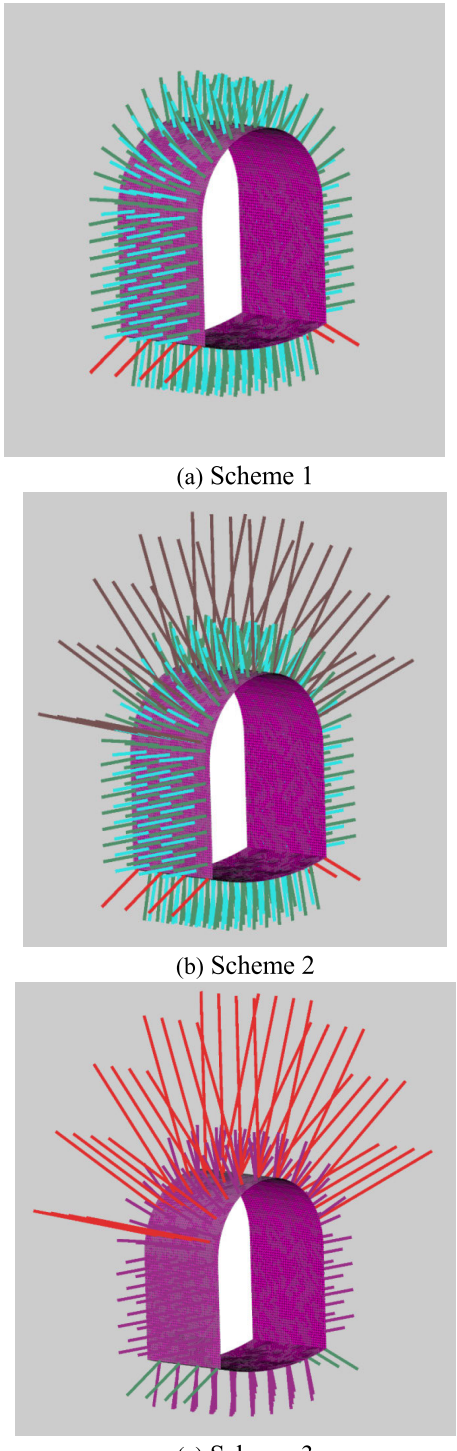

FIGURE 5. Model diagram of three support schemes.

Through the analysis and comparison of the surrounding rock displacement of the roadway, it can be seen that among the three support schemes, scheme 1 has the worst effect.

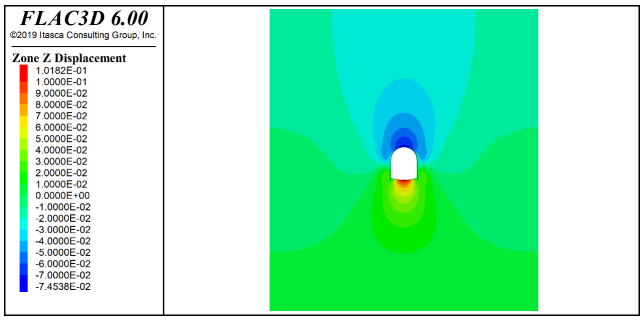

(a) Scheme 1

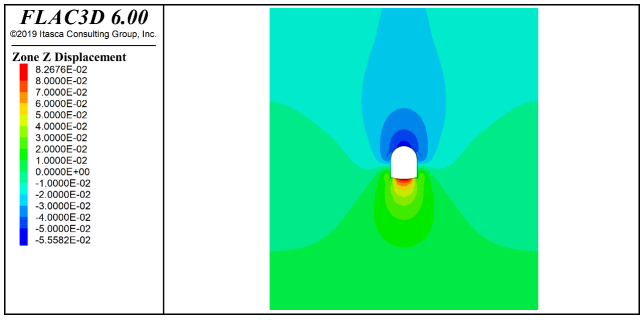

(b) Scheme 2

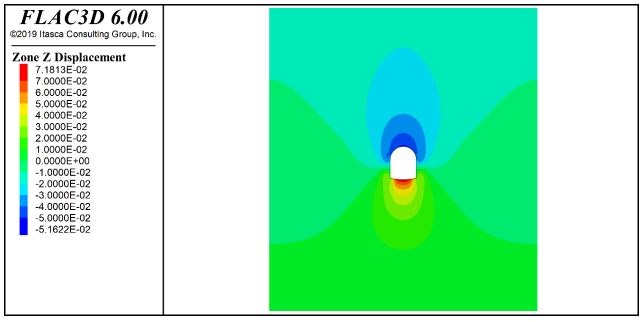

(c) Scheme 3

FIGURE 6. Three schemes of vertical displacement cloud map.

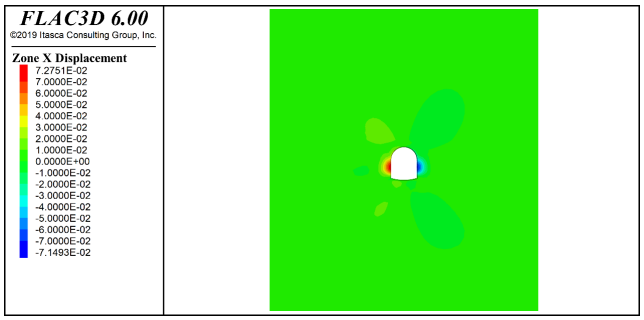

(a) Scheme 1

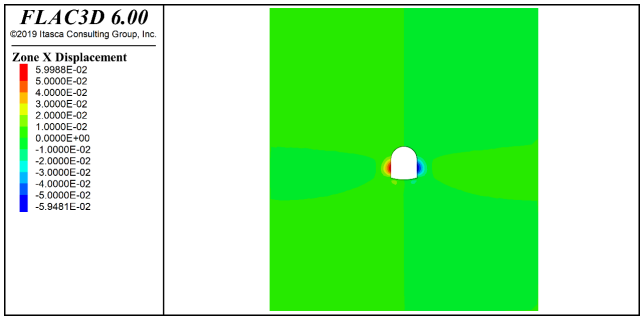

(b) Scheme 2

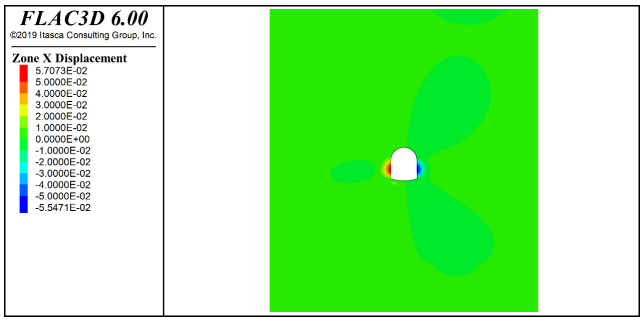

(c) Scheme 3

FIGURE 7. Three schemes of horizontal displacement cloud map.

The deformation of the roof and floor and the two sides is larger, and there is a risk of coal mine disasters such as slabs and roof fall. The supporting effect of the third scheme is better, which can basically guarantee the overall stability of the surrounding rock of the roadway. The deformation of the roof, floor and the two side of the roadway is controlled within a reasonable range, and the supporting effect of the scheme 3 is better than that of the scheme 2.

Combined with the above displacement analysis, the support effect of scheme 3 is better, which can ensure the stability of the roadway.

C. STRESS ANALYSIS OF ROADWAY SURROUNDING ROCK

1) VERTICAL STRESS

According to figure 8, the vertical stress distribution of surrounding rock under the three support schemes all present the following situation: stress concentration occurs in the surrounding rock on the surface of the two side of the roadway and the roof and floor, and the surrounding rock stress on the surface of the roadway changes greatly. At the same time, there is a pressure relief zone in the surrounding rock on the surface of the roadway, and the pressure relief zone on the roof is smaller than the floor. The maximum vertical stresses of the roof and floor surrounding rocks of the three schemes are 5.25 MPa, 4.15 MPa, and 3.65 MPa, respectively. The maximum stresses in the high stress concentration areas of the two sides of the roadway reach 41.6 MPa, 36.5 MPa, and 35.4 MPa, respectively. It can be seen that with bolt support with the reduction of the row spacing between the structures and the application of anchor cables, the surrounding rock stress in the high-stress zone of the roadway gradually decreases.

2) HORIZONTAL STRESS

Under the action of horizontal stress, it can be seen from figure 9 that arc-shaped pressure relief areas appear in the spur and bottom plate of the three support schemes. The maximum stress in the high stress concentration area of the

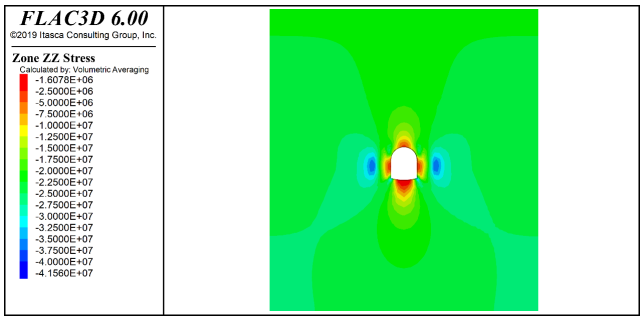

(a) Scheme 1

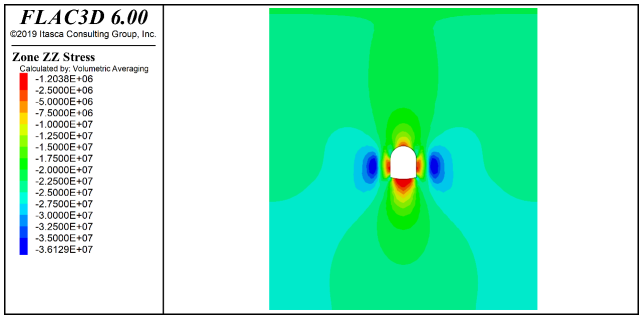

(b) Scheme 2

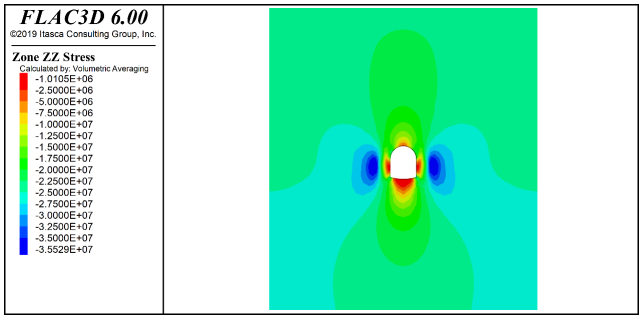

(c) Scheme 3

FIGURE 8. Three schemes of horizontal stress cloud map.

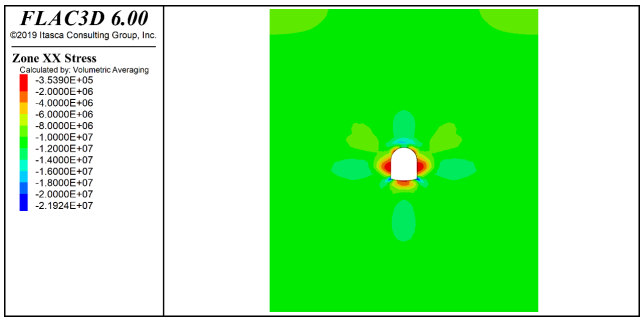

(a) Scheme 1

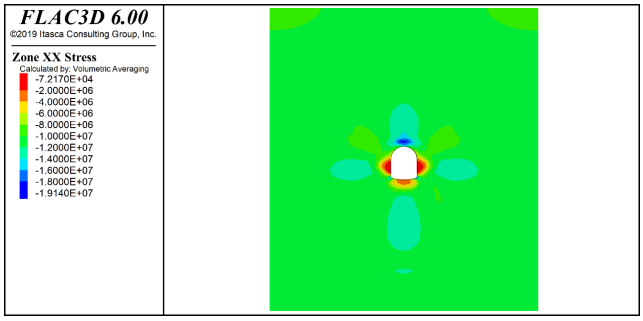

(b) Scheme 2

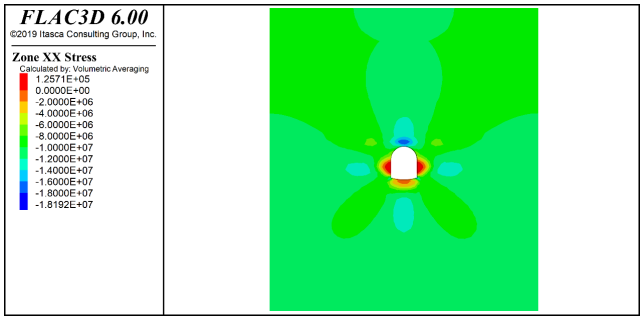

(c) Scheme 3

FIGURE 9. Three schemes of horizontal stress cloud map.

three support schemes reached 22.5 MPa, 19.2 MPa and 18.1 MPa respectively. The stress concentration phenomenon of scheme 2 and scheme 3 mainly occurs in the bottom corner. Compared with scheme 1, the stress release area of the two sides of the roadway and the floor surrounding rock becomes smaller. The stress release area on both sides of the vault gradually disappears and the surrounding rock stress It has been reduced and the supporting effect is good. It can be seen that the application of anchor cables and the increase of supporting density reduce (scheme 3) the horizontal stress of surrounding rock, and the supporting effect is better.

Combined with the above stress analysis, scheme 3 has a better support effect and can ensure the stability of the roadway.

D. STRESS ANALYSIS OF SUPPORTING STRUCTURE

Scheme 1 The maximum load that the anchor rod can bear is 197 MPa, and the bolts at the two sides of the roadway and bottom floor are more concentrated. In scheme 2, the maximum load of bolts and anchor cables is 296 MPa. After the anchor cable is added, the stress can be transferred to the surrounding rock by the anchor cables, which improves the stress condition of surrounding rock. Scheme 3 increases the supporting density and the length of the anchor cables and bolts, and the maximum load of the anchor cables and bolts increases from 296 MPa to 316 MPa. The force of the bottom floor bolts has also been significantly improved, and the force of the surrounding rocks is good, ensuring the stability of the roadway.

Combining the stress analysis of the above supporting structure, the supporting effects of the scheme 3 is better, which can meet the needs of safe use of the roadway.

E. SUPPORT SCHEME DETERMINATION

The surface displacement of the surrounding rock can directly reflect the support effect of the roadway and comprehensively

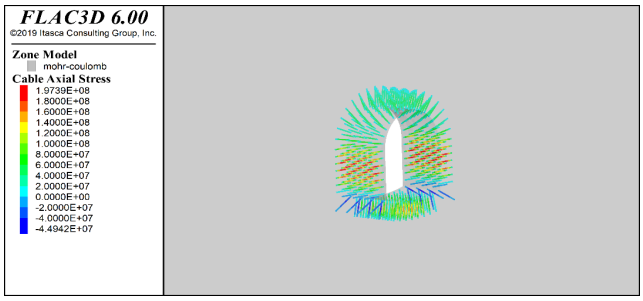

(a) Scheme 1

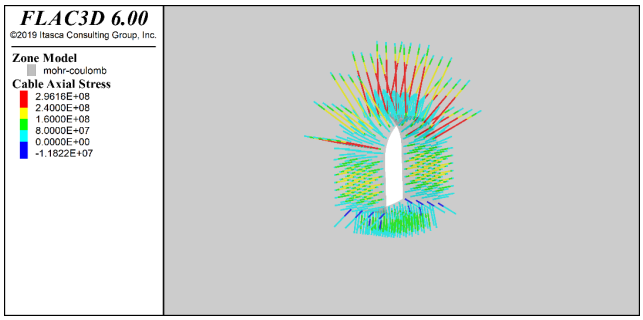

(b) Scheme 2

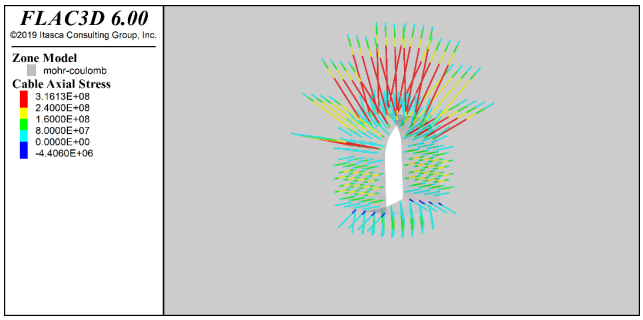

(c) Scheme 3

FIGURE 10. Three schemes of supporting structure stress cloud map.

reflect the stability of the surrounding rock. In order to deeply analyze the supporting effect of each supporting scheme, a detailed analysis of displacement and deformation should be carried out. The plotted top and bottom plates and the displacement of the two sides change with time, as shown in Figure 11.

The numerical simulation results of the above-mentioned schemes are further sorted out and shown in table 6, so as to judge the best scheme more intuitively.

Through the analysis and Research on the displacement, stress and supporting structure stress of the three design schemes, the feasibility of adopting full section support in roadway is verified. For the support effect of scheme 1, the surrounding rock of roadway still has large deformation, prone to rib spalling, roof fall and excessive deformation of floor, and the support effect is not ideal. After adding

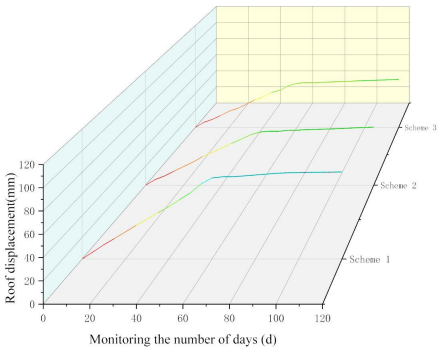

(a) Three support schemes roof displacement

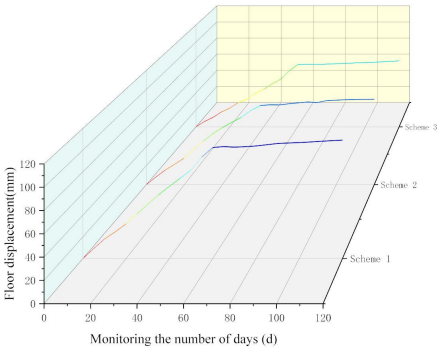

(b) Three support schemes floor displacement

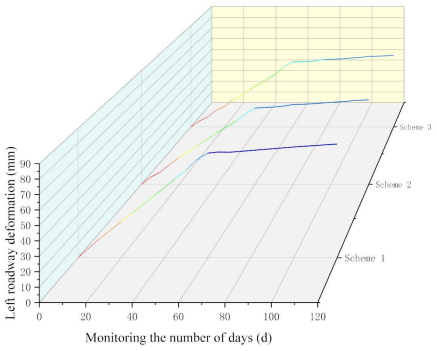

(c) Displacement of the left roadway of the three support schemes

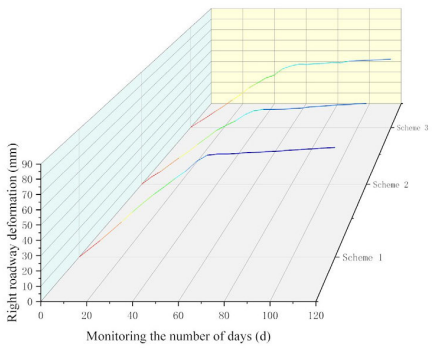

(d) Displacement of the right roadway of the three support schemes

FIGURE 11. Numerical simulation of displacement variation of each part of roadway with three support schemes.

TABLE 6. Comparative analysis of surrounding rock displacement of different schemes.

Support scheme	Floor displacement (mm)	Relative value	Roof displacement (mm)	Relative value	Displacement of two sides of the roadway (mm)	Relative value
Scheme 1	101.9	100%	74.5	100%	143.9	100%
Scheme 2	82.7	81.2%	55.6	74.6%	118.8	82.6%
Scheme 3	71.8	70.5%	51.7	69.4%	112.8	78.4%

anchor cable, scheme 2 and scheme 3 have achieved good supporting effect. Compared with scheme 1, the deformation of floor, the subsidence of roof and the approach of two sides in scheme 2 are reduced by 18.8%, 25.4% and 17.4% respectively, and the supporting effect has been significantly improved.

The stress of roadway surrounding rock surface is transferred from shallow to deep, and the stress of surrounding rock is more fully released, which meets the requirements of roadway support and normal use. After increasing the bolts support density and the length of anchor cables, the support effect of scheme 3 is improved. Compared with scheme 1, the floor deformation, roof subsidence and two sides of the roadway approach of scheme 3 are reduced by 29.5%, 30.6% and 21.6% respectively.

It can be seen from Figure 11 that the rate of change of displacement changes greatly at first, and begins to stabilize at about 50 or 60 days.

Therefore, based on the above analysis and consideration of surrounding rock displacement, stress and supporting structure stress, scheme 3 can ensure the stability of surrounding rock and the supporting effect is good. From the practical engineering construction and economic aspects, it is more economical to adopt scheme 3, which can ensure the normal use of the roadway, so it is proposed to adopt scheme 3 as the final support scheme.

V. SCHEME APPLICATION AND FIELD TEST EFFECT MONITORING

In order to determine the stability, convergence and feasibility of scheme 3 obtained by the numerical simulation method, scheme 3 was applied in the actual engineering construction of the mine tunnel. And to monitor its force and deformation data, in order to compare with the numerical simulation results.

A. SUPPORT SCHEME AND SUPPORT PARAMETERS

According to the actual engineering situation of the mine roadway, combined with the previous analysis results, scheme 3 is used as the final support scheme. The specific support parameters are as follows:

1) High-strength bolts on the roof and the two sides of the roadway

High-strength pre-stressed resin anchor rods with a diameter of 22 mm and a length of 2.4 m are used, and the row spacing is 700 mm.

2) Grouting bolts on the roof and the two sides of the roadway

A seamless grouting bolt with a diameter of 20 mm and a length of 2.2 m is used, with a row spacing of 1400 mm, and the resin anchor rod is spaced apart and arranged.

3) Anchor cable on the roof and the two sides of the roadway

A high-strength anchor cable with a diameter of 21.8 mm and a length of 9.6 m is used, and the row spacing is 1400 mm.

4) Shotcrete layer

Use ordinary concrete with strength C_{20} and thickness 150 mm.

5) Metal mesh

A metal mesh with a diameter of 6.5 mm and a grid density of 100 × 100 mm is used.

6) Steel ladder

A steel ladder with a diameter of 20 mm is used, and the resin bolt on the roof and the two sides of the roadway.

7) T-shaped steel belt

Specification GD II 140/20 mm.

8) Grouting

Ordinary cement slurry is selected as the grout, the grouting pressure is 1.5 MPa, and the final pressure is 2.5 MPa.

9) High-strength bolt

A high-strength pre-stressed resin bolt with a diameter of 22 mm and a length of 2.4 m is used, and the row spacing is 700 mm. The bolts are connected by a 140 mm wide T-shaped steel belt as a whole.

10) Grouting bolt on bottom floor

A seamless grouting bolt with a diameter of 20 mm and a length of 2.2 m is used, with a row spacing of 1400 mm, and the resin bolt is spaced apart and arranged.

B. FIELD MONITORING PROGRAM

Field monitoring: that is, monitoring in accordance with the requirements in the actual construction of the project. In this study, it refers to real-time monitoring of the force and displacement of the surrounding rock of the roadway. This monitoring is carried out on the spot, not a numerical simulation.

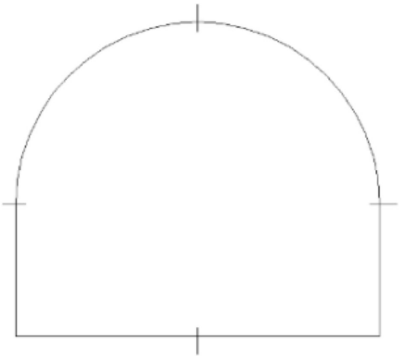

FIGURE 12. Arrangement of measuring points on the surface displacement of surrounding rock.

In order to better optimize the design of the support plan and effectively guide the field construction, a 50 m long test section was selected, the initial support was monitored in real time, and the monitoring data was analyzed and compared. In order to optimize the support design, determine whether the construction technology and support plan are reasonable, and provide a basis for subsequent construction guidance.

In order to study the deformation characteristics of the surrounding rock after excavation, the deformation of the surrounding rock of the roadway was monitored and recorded in real time, so as to explore the change law of the surface displacement of the surrounding rock of the roadway over time. The measuring rod and the measuring gun are used to measure the surface displacement of the surrounding rock. Three monitoring sections are arranged, each with an interval of 20m, and its interruption surface 1 is close to the working surface. For the three monitoring sections, 4 measuring points are set by the mid-waist cross point method, that is, one measuring point is arranged at each of the roof and floor and the two sides of the section (Figure 12).

C. ANALYSIS OF MONITORING RESULTS

Figure 13 is analyzed as follows:

1) Rate of displacement change

It can be seen that the rate of change of the surface displacement of the surrounding rock of the roadway gradually decreases with the increase of the number of observation days.

The change process can be divided into the following stages:

The first is the severe deformation stage. About 2-10 days after the excavation of the roadway, the roadway surface displacement change rate increased rapidly. During this period, the average change rate of the surrounding rock surface displacement reached 8.4 mm/d, and the maximum change rate reached 10.5 mm/d. The reason is that the normal stress of the surrounding rock surface is unloaded after the excavation of the roadway. The tangential stress increases due to the redistribution of the stress. The deformation of the surrounding rock surface is transferred from the shallow part to the deep part, and the displacement amount and the displacement change rate of the surrounding rock increase rapidly.

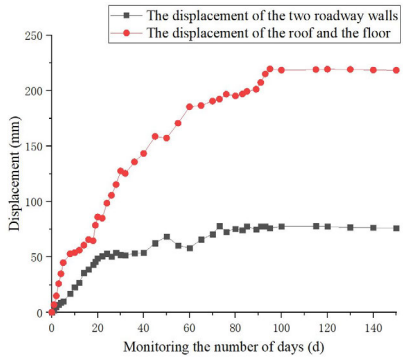

(a) Monitoring section 1

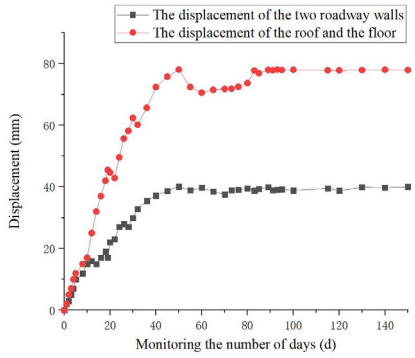

(b) Monitoring section 2

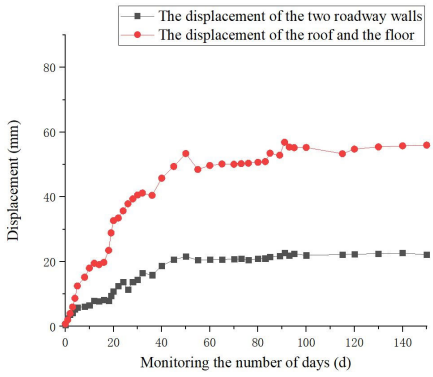

(c) Monitoring section 3

FIGURE 13. Monitoring results of three monitoring sections.

The second is the wave deformation stage. About 10-60 days after the excavation of the roadway, the rate of change of the surface displacement of the surrounding rock of the roadway fluctuates. The reason is that the monitoring section is close to the tunneling face, and the surrounding rock of the roadway is affected by the excavation disturbance of the face. When the roadway was excavated for about 50 days, the rate of change of the surface displacement of the surrounding rock of the three monitored sections increased

suddenly and significantly. The reason is that the normal stress on the surface of surrounding rock is unloaded after the roadway excavation. The tangential stress increases due to the redistribution of stress. The deformation of surrounding rock surface is transferred from shallow to deep, and the displacement and displacement change rate of surrounding rock increase rapidly.

The last is the stable deformation stage. After the excavation of the roadway exceeds 60 d, the surface displacement rate of the surrounding rock of the roadway is less than 1 mm/d to reach the stable stage.

2) The amount of displacement change

The maximum convergence deformation of roof, floor and two sides of roadway in section 1 are 218.7 mm and 84.1 mm respectively. The maximum convergence deformation of roof, floor and two sides of roadway in section 2 are 76.9 mm and 42.5 mm respectively. The maximum convergence deformation of roof, floor and two sides of roadway of section 3 are 55.3 mm and 20.8 mm respectively. It can be seen that section 1 is close to the working face, which is easily affected by the excavation disturbance of the working face, and its displacement is large.

Figure 13 shows that the convergent deformations of the surrounding rock surfaces of the three monitoring sections are the roof and floor of the roadway with the largest deformation, and the two sides of the roadway have the smallest deformation. Generally speaking, in the process of roadway support, the roof and the two sides of the roadway are supported first. If the floor is left unsupported for a long time, it is easy to cause stress concentration and cause serious deformation of the bottom plate. For deep mine large section roadways, the deformation of the floor is large and lasts for a long time, and it will affect the stability of the roadway roof and the two sides of the roadway, which may eventually cause the overall instability of the roadway.

D. COMPARISON OF FIELD MONITORING RESULTS AND NUMERICAL SIMULATION RESULTS

Analyzing and comparing the roadway displacement calculation results obtained by numerical simulation of scheme 3 (Table 6) in the previous article with the roadway surface displacement monitoring results in field monitoring in this chapter (Figure 13), the following conclusions are obtained:

(1) The field monitoring results show that after the excavation of the roadway exceeds 60 days, the surface displacement of the roadway surrounding rock gradually reaches a stable stage, which is basically consistent with the trend of the roadway surrounding rock displacement curve obtained by the numerical simulation. The numerical simulation result of scheme 3 is obtained Although the deformation of the surrounding rock of the roadway is different from the deformation of the surrounding rock of the roadway obtained by field monitoring, the difference is small.

(2) When the roadway was excavated for about 50 days, the rate of change of the surface displacement of the surrounding rock of the three monitoring sections all increased suddenly and significantly, which was not reflected in the numerical simulation results. The reason for this phenomenon is that the excavation of the adjacent roadway at about 50 days redistributes the stress of the surrounding rock, resulting in stress concentration. The original fracture zone in the surrounding rock continues to expand, and the rate of change of the surface displacement of the surrounding rock of the roadway is sudden. In addition, such field construction factors were not involved in the numerical simulation.

(3) The surrounding rock displacement changes of the three monitoring sections all show the distribution law of ''the right side is smaller than the left side and the left side is smaller than the roof'', which is similar to the law presented by the numerical simulation calculation results of scheme 3.

(4) There is a certain difference between the field monitoring results of the roof and floor displacements of section 1 and the numerical simulation results. The reason is that the monitoring section and the driving face are close to each other, and the surrounding rock of the roadway is affected by the excavation disturbance of the working face.

The reasons for the difference between the field monitoring results of the roadway displacement on both sides of section 3 and the numerical simulation results are:

a) With the excavation and support of the roadway, part of the deep rock mass is less broken. After the support, the rock mass has formed a whole with the supporting structure, which has strong stability and low deformation.

b) Numerical simulation itself cannot completely simulate the real situation, and there are certain errors.

(5) CPU calculation time (taking displacement calculation as an example): In the numerical simulation process, due to different conditions (such as test position and stress state), the calculation complexity is different. Therefore, CPU computation time varies greatly. In this case, the CPU calculation time of the computer is not a reference, but a stable displacement over a long period of time is used as the basis for judging convergence. In this study, a stable displacement that meets the standard is the most important basis for engineering safety. Therefore, the CPU calculation time is no longer listed.

Through the comparative analysis of the numerical simulation results and the field monitoring data, it is not difficult to find that the two are not completely consistent. However, the variation law of the surrounding rock displacement of the roadway shown by the numerical simulation is basically the same as the variation law obtained from the field monitoring, and the variation of the surrounding rock displacement of the roadway obtained by the two is not much different. This is because the rock mass is regarded as isotropic during the numerical simulation calculation and the influence of actual conditions such as groundwater is not considered. During the field construction process, it will also be interfered by construction and other factors, and the actual working conditions cannot be fully and accurately simulated. There will be some differences between the results obtained by the two, but in general, the results of mine pressure monitoring verify

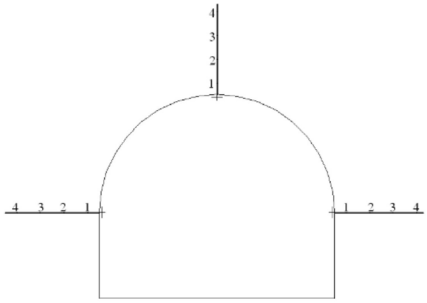

FIGURE 14. Multi-point displacement measurement point layout drawing.

the accuracy of the numerical simulation calculation and the feasibility of scheme 3.

VI. DISCUSSION

Monitoring the change of surrounding rock displacement should not only stop at the surface of surrounding rock. The deformation of surrounding rock in deeper surrounding rock areas may also affect the stability of surrounding rock, thereby affecting engineering safety. In order to explore the surrounding rock deformation in the deeper area and ensure that no further damage occurs over time, it is necessary to monitor the surrounding rock deformation in the deeper surrounding rock area.

A. VARIATION LAW OF DEEP SURROUNDING ROCK DISPLACEMENT WITH TIME

In order to study the displacement changes of the deep surrounding rock after excavation, the displacement of the deep surrounding rock of the roadway was monitored and recorded. The multi-point displacement meter is used to monitor the displacement of the surrounding rock in the deep part of the roadway, and three monitoring sections are set up, each with an interval of 20 m. Each monitoring section is arranged with 3 measuring holes, which are arranged on the vault and the two sides (Figure 14). Each measuring hole is set with 4 measuring points. The distance between each measuring point and the surrounding rock surface is 2 m, 4 m, 6 m, 8 m, the measuring point at the bottom of the hole is placed in the deep stable rock formation.

It is one of the important means to verify the feasibility of support scheme to measure the displacement of deep surrounding rock by multi-point displacement meter. The displacement variation of the three measuring holes with time is shown in Figure 15-17.

1) CHANGE RATE OF DISPLACEMENT OF DEEP SURROUNDING ROCK

After the excavation, the displacement of deep surrounding rock increases, but the increase degree of each point is different. Generally speaking, the change rate gradually decreases with the increase of time. According to the monitoring data, the displacement change process is divided into the following stages:

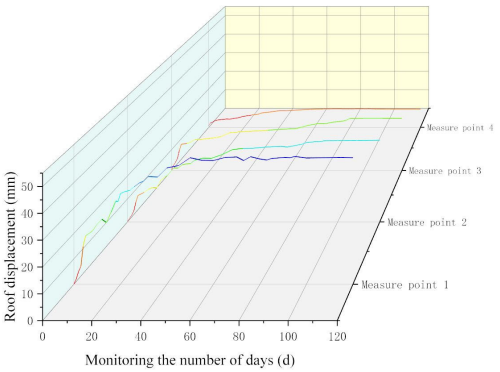

(a) Roof measuring hole

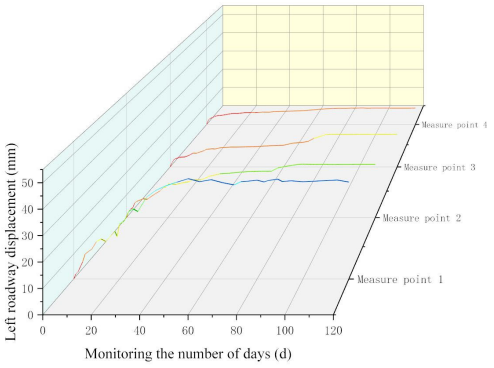

(b) Measuring hole of left side of roadway

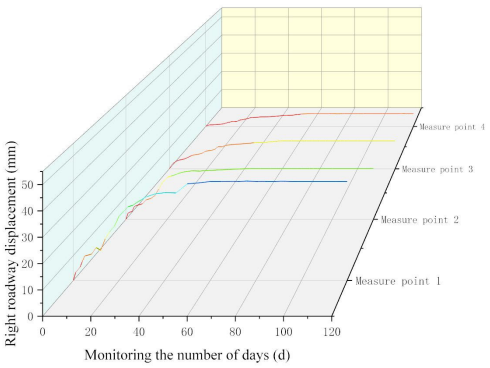

(c) Measuring hole on right side of roadway

FIGURE 15. Relationship between displacement and time at different depths of section 1.

The first is the stage of severe deformation. About 2-20 days after excavation, the deformation rate of deep surrounding rock increases rapidly, and the maximum deformation rates of vault, left side and right side are 6.5 mm/d, 3.9 mm/d and 3.1 mm/d respectively.

The second stage is wave deformation. About 20-60 days after the excavation, the influence of excavation disturbance on the surrounding rock gradually weakened. However, when the roadway is excavated for about 50 days, the deformation

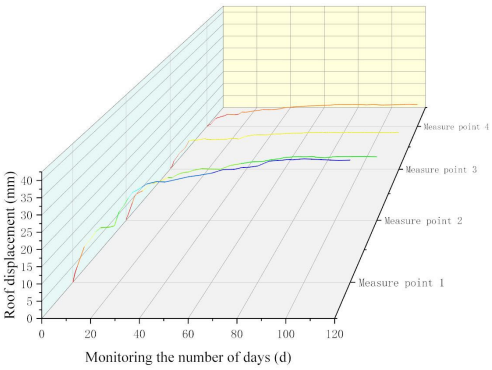

(a) Roof measuring hole

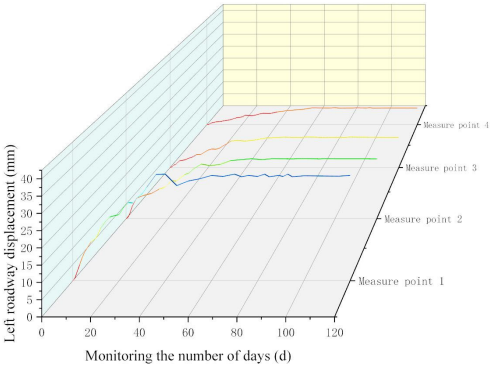

(b) Measuring hole of left side of roadway

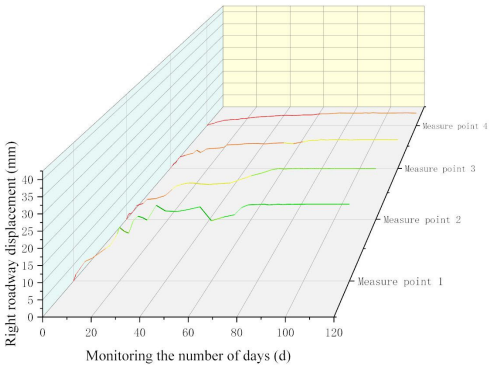

(c) Measuring hole on right side of roadway

FIGURE 16. Relationship between displacement and time at different depths of section 2.

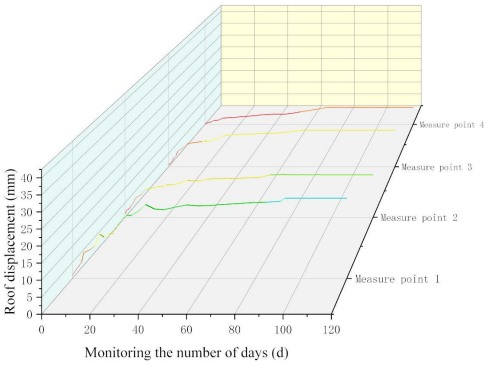

(a) Roof measuring hole

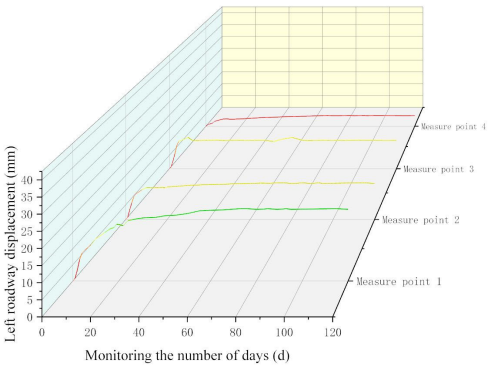

(b) Measuring hole of left side of roadway

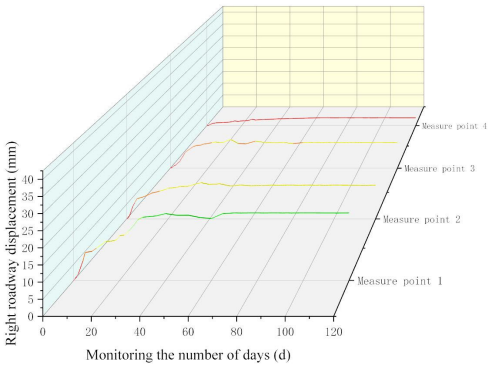

(c) Measuring hole on right side of roadway

FIGURE 17. Relationship between displacement and time at different depths of section 3.

rate of the deep surrounding rock increases suddenly due to the excavation disturbance of the adjacent roadway, which is the same as that of the roadway surface displacement at the same time.

Finally, the stable deformation stage. After excavation for more than 60 days, the strain rate is less than 1 mm/d, which indicates that the combined support of bolt and grouting has obvious effect and the deformation of surrounding rock is basically controlled.

2) VARIATION OF DISPLACEMENT OF DEEP SURROUNDING ROCK

Through the analysis of figure 15-17, combined with table 7 and table 8, it can be seen that the deep displacement variation of surrounding rock of these three sections shows the distribution law of ''the right side is less than the left side, and the left side is less than the roof''. The reason for this distribution law is that the left side of the roadway is adjacent to the fault, resulting in the increase of the displacement change

TABLE 7. Monitoring Results of Measuring Points at 2m in Different Sections and Holes.

Section	Roof (mm)	Left side of roadway (mm)	Right side of roadway (mm)
1	49.8	40.4	39.7
2	37.4	32.2	23.6
3	24.9	22.1	10.8

TABLE 8. Monitoring Results Of Measuring Points At 8m In Different Sections And Holes.

Section	Roof (mm)	Left side of roadway (mm)	Right side of roadway (mm)
1	9.6	7.3	6.4
2	8.8	6.7	5.1
3	6.9	4.3	3.2

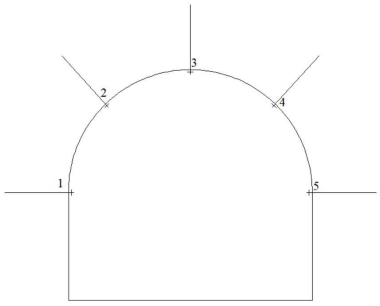

FIGURE 18. Layout of anchor rod axial force measuring points.

amount and change rate of the surrounding rock of the left side. When the two sides of the roadway are excavated, the deformation of surrounding rock and the disturbed stress field are superimposed, which makes the stress disturbed area of the roof increase and the displacement of the side is less than that of the roof.

The reason for the above phenomenon is that there will be a high degree of stress concentration after the excavation of large cross-section roadway in deep mine, and because of the complex geological conditions, the surrounding rock of roadway will be affected by faults, the integrity of rock mass will be damaged, and the strength will be reduced. At this time, the range of stress disturbance area and plastic failure area is wide, and it will continue to expand from the surface of surrounding rock to the deep.

To sum up, the deformation law of surrounding rock in deeper surrounding rock area is similar to that of surrounding rock surface. These are basically consistent with the analysis in section V (C), and is also in good agreement with Wu's [8] research conclusion, which fully illustrates the feasibility

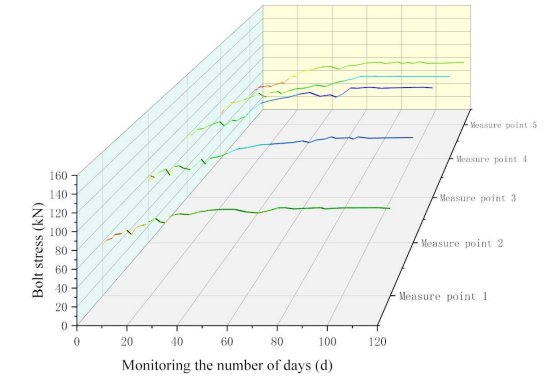

(a) Section 1

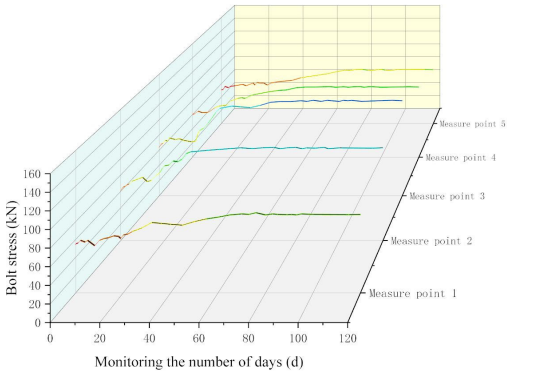

(b) Section 2

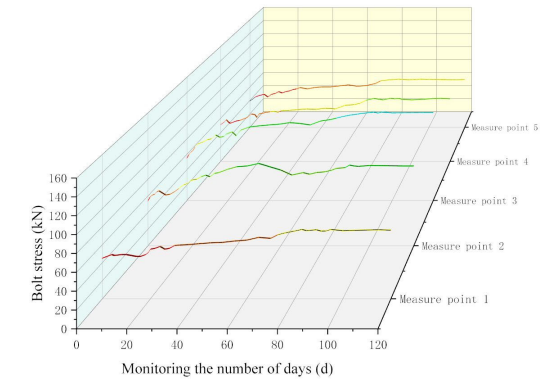

(c) Section 3

FIGURE 19. Stress time curves of bolts with different sections.

of the numerical simulation method and the correctness of scheme 3.

B. VARIATION LAW OF BOLT AXIAL FORCE WITH TIME

In order to fully understand the supporting effect of bolt and explore the change of bolt axial force, the change of bolt axial force is monitored and recorded. The bolt dynamometer (20t type) is used to measure the axial force of the anchor rod. Three monitoring sections are set, each with a distance of 20 m. The arrangement of the measuring points of the

three sections is shown in Figure 18. From left to right, it is recorded as measuring point 1, measuring point 2, measuring point 3, measuring point 4 and measuring point 5.

Figure 19 shows the variation of axial force of anchor rod with time.

1) CHANGE RATE OF BOLT AXIAL FORCE

The change rate of the axial force of the anchor rod gradually decreases with the increase of the observation days. The specific change process can be divided into the following stages:

The first is the rapid increase phase. About 2-10 days after excavation, the change rate of bolt axial force increases rapidly. The reason for this phenomenon is that roadway excavation will unload the normal stress on the surface of surrounding rock, and the deformation of surrounding rock will increase rapidly. The construction of the anchor can control the deformation of the surrounding rock, and the initial prestress of the anchor can inhibit the fracture and expansion of the surrounding rock to a certain extent, so the axial force of the anchor will increase rapidly at this time. In this stage, the axial force of local anchor also decreased. The reason for this phenomenon is that the bolt tray and its surrounding rock fall off due to the blasting construction of the front heading face.

The second is the fluctuation stage. About 10-60 days after excavation, the curve of bolt axial force versus time fluctuates up and down. The reason for this phenomenon lies in the repeated process of compression and rebound in the surrounding rock caused by the construction of supporting structure, so the axial force of bolt is also changing. When the excavation time is about 50 days, the surrounding rock of the roadway is affected by the excavation disturbance of the adjacent roadway, and the axial force of the bolt changes suddenly, which is the same as the change rate of the surface displacement and the deep displacement of the surrounding rock at the same time.

The last stage is the stable stage. After about 60 days of roadway excavation, the pressure difference between the two consecutive measurements is less than 0.1 kn, and the change of bolt axial force tends to be stable.

2) VARIATION OF BOLT AXIAL FORCE

Section 1 is close to the head of the working face, which is easily affected by the excavation disturbance of the working face. The five measuring points (3, 2, 4, 1, 5) are arranged from large to small according to the maximum anchor axial force, which are 143 kN, 127 kN, 115 kN, 97 kN, 93 kN respectively. The five measuring points (3, 2, 4, 1, 5) of section 2 are arranged from large to small according to the maximum bolt axial force, which are 125 kN, 113 kN, 99 kN, 88 kN and 81 kN respectively. The five measuring points (3, 2, 4, 1, 5) of section 3 are 114 kN, 96 kN, 87 kN, 76 kN and 71 kN respectively according to the maximum bolt axial force.

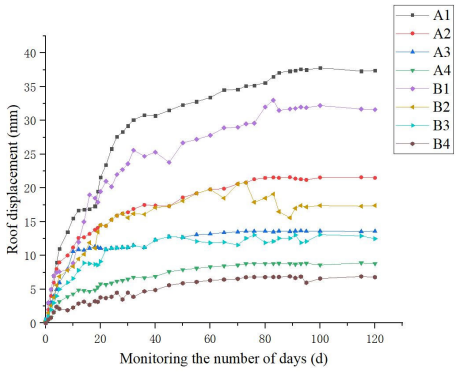

Note: A1-A4 is the field monitoring results, B1-B4 is the numerical simulation results.

FIGURE 20. Comparison of actual monitoring and numerical simulation results of displacement at different depths of roof measuring hole in Section 2.

Here, 2 and 4 measuring points are regarded as roadway shoulder. It can be seen from Figure 19 that the axial force of the bolts of the three sections changes with time, showing the distribution law of ''the roof is greater than the two shoulders, the two shoulders are greater than the two sides of the roadway''. The reason for this law is that the bolts can limit the deformation of the surrounding rock, and the axial force of the bolts will change with the deformation of the surrounding rock.

C. COMPARED WITH THE NUMERICAL SIMULATION RESULTS

In order to verify the above rules, the measuring points are also arranged according to Figure 14 and Figure 18 in the numerical simulation software, and the displacement changes at different depths and the stress conditions of the bolt are detected. Because of the space, the results will not be listed one by one here. Only taking the displacement at different depths of the measuring hole of section 2 roof as an example, the actual monitoring and numerical simulation results are compared.

It can be seen from Figure 20 that the field monitoring and numerical simulation results are not completely consistent. However, the change pattern in the displacement of the surrounding rock of the roadway shown by the numerical simulation are basically the same as those obtained from the field monitoring, and the amount of the displacement of the surrounding rock of the roadway obtained by the two is not much different.

In addition, the displacement changes of the field monitoring results are all small, and they all meet the engineering safety construction standards, which can further illustrate the reliability of scheme 3. These are basically consistent with the analysis in section V (C), and is also in good agreement with Wu's [8] research conclusion (the results of numerical simulation and on-site monitoring are more consistent), which

fully illustrates the feasibility of the numerical simulation method and the correctness of scheme 3.

VII. CONCLUSION

Aiming at the high buried and deep roadway, its geological profile was explored, and based on FDM, combined with FLAC^{3D} software, the reason for its stress and deformation was analyzed theoretically. Three support schemes were designed through PDM, and the force and deformation under different schemes were simulated through FLAC^{3D} software. The comparative analysis obtained the optimal support plan. The optimal support plan is applied to the actual project, and field monitoring is carried out. The monitoring results are in good agreement with the numerical simulation results. The specific conclusions are as follows:

(1) The deformation and failure characteristics of the mine roadway are briefly analyzed: the bottom heave phenomenon is serious; the brittle-extended transformation characteristics; the large deformation and strong rheological characteristics. The main factors affecting deformation and failure are summarized: rock fractures, low rock strength, impact of buried depth, impact of groundwater, impact of ground temperature changes, unreasonable supporting structure, and construction factors.

(2) In the unsupported state after excavation, the maximum deformation of the left and right sides of the roadway reached 1583 mm and 1627 mm, and the maximum displacements of the roof and floor were 1291 mm and 473 mm. This shows that if the initial support treatment is not carried out in time after the excavation of the roadway, it will soon be subjected to the pressure of the surrounding rock and produce large deformation, so that the roadway will collapse and damage.

(3) Considering multiple factors, 3 new support schemes are designed. Comparing the analysis and research of the displacement, stress and supporting structure force of the three design schemes and actual engineering factors, scheme 3 has the smallest displacement of surrounding rock, the smallest stress in the stress concentration area, and the largest structural stress, which verifies the coal mine roadway the feasibility of adopting full-face support, scheme 3 is proposed as the optimal support plan. Scheme 3 is actually applied and monitored. The monitoring effect is not much different from the numerical simulation results and the rules are similar. This further illustrates the feasibility of the method of designing the support scheme through FLAC^{3D} software combined with PDM.

(4) Through monitoring the deformation of surrounding rock at different depths, it is found that the surrounding rock deformation presents three stages over time: severe deformation stage, fluctuating deformation stage, and stable deformation stage, which are similar to the aforementioned surrounding rock surface deformation law. Each measuring point reaches a stable state within the monitoring time, which further illustrates the feasibility of scheme 3.

(5) About 2-10 days after the excavation of the roadway, the relationship curve between the bolt axial force and time rises rapidly. About 10-60 days after the excavation of the roadway, the relationship between the bolt axial force and time fluctuates up and down. About 60 days after the excavation of the roadway, the difference between the pressure values measured twice in succession was no more than 0.1 kN, and the axial force of the bolt tended to be stable. The axial force of the bolts of the three sections changes with time, showing the distribution law of ''the roof is larger than the two shoulders of the roadway, and the two shoulders of the roadway are larger than the two sides of the roadway''.

(6) Although the change law of the surrounding rock displacement of the roadway presented by the numerical simulation is not exactly the same as the change law obtained from the field monitoring, the basic law is the same. The displacement change of the surrounding rock of the roadway obtained by the two methods is also not much different. Overall, the results of mine pressure monitoring verify the accuracy of numerical simulation calculations and the feasibility of scheme 3. It also provides theoretical basis and technical guidance for engineering hypothesis under approximate conditions.

REFERENCES

[1] M. G. B. Atia, H. El-Hussieny, and O. Salah, ''A supervisory-based collaborative obstacle-guided path refinement algorithm for path planning in wide terrains,'' *IEEE Access*, vol. 8, pp. 214672–214684, 2020, doi: 10.1109/ACCESS.2020.3041802.

[2] B.-O. Tak and J.-S. Ro, ''Analysis and design of an axial flux permanent magnet motor for in-wheel system using a novel analytical method combined with a numerical method,'' *IEEE Access*, vol. 8, pp. 203994–204011, 2020, doi: 10.1109/ACCESS.2020.3036666.

[3] A. Kaneko, Y. Hayashi, T. Anegawa, H. Hokazono, and Y. Kuwashita, ''Evaluation of an optimal radial-loop configuration for a distribution network with PV systems to minimize power loss,'' *IEEE Access*, vol. 8, pp. 220408–220421, 2020, doi: 10.1109/ACCESS.2020.3043055.

[4] Z. Tian, S. Jing, W. Liu, S. Gao, and J. Zhang, ''Experimental and numerical study on cutting performance of coal plow,'' *IEEE Access*, vol. 8, pp. 211882–211891, 2020, doi: 10.1109/ACCESS.2020.3039438.

[5] J. Lei, B. Xue, H. Fang, Y. Li, and M. Yang, ''Forward analysis of GPR for underground pipes using CUDA-implemented conformal symplectic euler algorithm,'' *IEEE Access*, vol. 8, pp. 205590–205599, 2020, doi: 10.1109/ACCESS.2020.3037811.

[6] J. Tabatabaei, M. S. Moghaddam, and J. M. Baigi, ''Rearrangement of electrical distribution networks with optimal coordination of grid-connected hybrid electric vehicles and wind power generation sources,'' *IEEE Access*, vol. 8, pp. 219513–219524, 2020, doi: 10.1109/ACCESS.2020.3042763.

[7] M. Tahkola, J. Keranen, D. Sedov, M. F. Far, and J. Kortelainen, ''Surrogate modeling of electrical machine torque using artificial neural networks,'' *IEEE Access*, vol. 8, pp. 220027–220045, 2020, doi: 10.1109/ACCESS.2020.3042834.

[8] Y. Wu, W. Qiao, S. Zhang, Z. Zhang, Y. Li, Z. Fan, and L. Zhang, ''Application of computer simulation method in deep underground engineering of complicated geological condition,'' *IEEE Access*, vol. 8, pp. 174943–174963, 2020, doi: 10.1109/ACCESS.2020.3025907.

[9] Y. Wu, X.-X. Yang, and D.-K. Sun, ''Experimental investigation of the mechanical behaviors of brittle rock materials containing en echelon boreholes,'' *Arabian J. Geosci.*, vol. 13, no. 11, pp. 1–13, Jun. 2020, doi: 10.1007/s12517-020-05440-5.

[10] X. L. Du, ''The influence of the number of cables in FLAC (3D) on the results of the bolt pulling simulation test,'' *Coal Mine Saf.*, vol. 51, no. 7, pp. 215–220, 2020, doi: 10.13347/j.cnki.mkaq.2020.07.045.

[11] Z. Chao, S. Weidong, F. Jianxin, L. Yang, and Z. Kaicheng, ''Study on the treatment technology of broken rock mass roadway in submarine gold mines,'' *J. Mining Rock Control Eng.*, vol. 2, no. 3, pp. 48–55, 2020, doi: 10.13532/j.jmsce.cn10-1638/td.20200313.002.

[12] L. Jintao, C. Hongtao, L. Weixing, and G. Yongchao, "Study on the stability of bottom structure based on FLAC (3D) numerical simulation," *Mining Res. Develop.*, vol. 40, no. 4, pp. 19–23, 2020, doi: 10.13827/j.cnki.kyyk.2020.04.004.

[13] Z. J. Yanli and W. Yongping, "Research on deformation and failure mechanism and support technology of stoping roadway in steep coal seam repeated mining," *Coal Eng.*, vol. 52, no. 2, pp. 91–95, 2020, doi: 10.11799/ce202002020.

[14] W. Shanyuan, Z. Qingwen, Y. Ming, L. Tingchun, X. Qingguo, and G. Hongyun, "Limestone roof roadway support technology in Qiuji coal mine," *Coal Mine Saf.*, vol. 51, no. 12, pp. 93–99, 2020, doi: 10.13347/j.cnki.mkaq.2020.12.017.

[15] H. Fei, "Study on numerical simulation of supporting technology for soft fractured rock mass bottom structure," *Mining Res. Develop.*, vol. 40, no. 5, pp. 94–97, 2020, doi: 10.13827/j.cnki.kyyk.2020.05.015.

[16] Q. Y. W. He and W. Zhixiu, "Analysis of instability mechanism and treatment of deep broken and weatherable roadways," *China Mining*, vol. 29, no. S1, pp. 388–393, 2020, doi: 10.12075./j.isn.1004-4051.2020.S1.069.

[17] Y. Du, G. Feng, Y. Zhang, X. Zhang, Y. Zhai, and J. Bai, "Pressure reduction mechanism and effect of working face passing through abandoned roadway by roof presplit," *Energy Sci. Eng.*, vol. 8, no. 10, pp. 3502–3513, Oct. 2020, doi: 10.1002/ese3.760.

[18] C. Zhu, Y. Yuan, Z. Chen, Z. Liu, and C. Yuan, "Study of the stability control of the rock surrounding double-key strata recovery roadways in shallow seams," *Adv. Civil Eng.*, vol. 2019, pp. 1–21, Aug. 2019, doi: 10.1155/2019/9801637.

[19] Y. Chao, L. Fan, C. Jianfeng, and W. Weijun, "Numerical simulation of the supporting effect of anchor rods on layered and nonlayered roof rocks," *Adv. Civil Eng.*, vol. 2020, Jan. 2020, Art. no. 4841658, doi: 10.1155/2020/4841658.

[20] W. HaiTao, C. Tong, W. YaJun, L. Tao, and Q. N. Hua, "Research of mechanical characteristics and roadway support in two-soft and one-hard coal seam," in *Proc. Int. Conf. Green Buildings Environ. Manage.*, vol. 186, 2018, Art. no. 012032, doi: 10.1088/1755-1315/186/5/012032.

[21] F. Pelli, P. K. Kaiser, and N. R. Morgenstern, "Effects of rock mass anisotropy and non-linearity on the near face stresses in deep tunnels," *Rock Mech. Rock Eng.*, vol. 28, no. 2, pp. 125–132, 1995, doi: 10.1007/BF01020065.

[22] B. Jianbiao, W. Xiangyu, and Y. Zhe, "Research on coupling support of high-stress soft rock roadway," *J. China Univ. Mining Technol.*, vol. 36, no. 4, pp. 421–425, 2007. [Online]. Available: https://kns.cnki.net/kcms/detail/detail.aspx?FileName=ZGKD200704000&DbName=CJFQ2007

[23] L. Dawei, H. Chaojiong, and B. Jianbiao, "Control mechanism and application of secondary supporting roadway with large rigidity and high strength," *Chin. J. Geotech. Eng.*, vol. 30, no. 7, pp. 1072–1078, 2008. [Online]. Available: http://kns.cnki.net/kcms/detail/detail.aspx?FileName=YTGC200807024&DbName=CJFQ2008

[24] L. Shucai, W. Hanpeng, Q. Qihu, L. Shuchen, F. Qingzhong, Y. Liang, X. Junhua, and Z. Qingsong, "Survey on the field monitoring of the fracture phenomenon of surrounding rocks in deep roadways," *Chin. J. Rock Mech. Eng.*, vol. 27, no. 8, pp. 1545–1553, 2008. [Online]. Available: http://kns.cnki.net/kcms/detail/detail.aspx?FileName=YSLX200808005&DbName=CJFQ2008

[25] L. Zhonghua, J. Xueyan, and Y. Wenxin, "Study on the brittle-ductile transformation characteristics of deep rock mass and the plastic limit state of overlying rock," *J. Liaoning Tech. Univ. (Natural Sci. Ed.)*, vol. 29, no. 6, pp. 1013–1015, 2010. [Online]. Available: http://kns.cnki.net/kcms/detail/detail.aspx?FileName=FXKY201006002&DbName=CJFQ2010

[26] X. Dongjun, "Rheological properties and long-term strength measurement of weak rock masses," *Rock Soil Mech.*, vol. 1, no. 1, pp. 37–50, 1980, doi: 10.16285/j.rsm.1980.01.003.

[27] L. Peng. *Deep Well Matoumen Coupling Support and Surrounding Rock Stability Analysis*. Shandong University of Science and Technology. Accessed: 2017. [Online]. Available: https://nxgp.cnki.net/kcms/detail?v=3uoqIhG8C475KOm_zrgu4lQARvep2SAk-6BvX81hrs37AaEFpExs0MzZi-_2LMBgkufxC8QDJGIymHGeC_JI-k6GJNgXbpeU&uniplatform=NZKPT

[28] G. Jianwei, "Deep well jointed surrounding rock roadway failure mechanism and control technology," *J. China Coal Soc.*, vol. 37, no. 9, pp. 1559–1563, 2012, doi: 10.13225/j.cnki.jccs.2012.09.028.

[29] L. Haiyan, L. Duanju, S. Qingguo, W. Huaixin, and L. Yuping, "Research on the failure mechanism and support technology of soft rock roadway in one thousand meters deep mine," *J. Shandong Univ. (Eng. Sci. Ed.)*, vol. 39, no. 4, pp. 112–115, 2009. [Online]. Available: http://kns.cnki.net/kcms/detail/detail.aspx?FileName=SDGY200904026&DbName=CJFQ2009

[30] W. Ruqiu, "High-stress soft rock roadway failure mechanism and support theory research," *Shanxi Archit.*, vol. 33, no. 26, pp. 142–143, 2007. [Online]. Available: http://kns.cnki.net/kcms/detail/detail.aspx?FileName=JZSX200726087&DbName=CJFQ2007

[31] S. Peide and Z. Cuiqi, "Study on geothermal field of surrounding rocks in deep mine roadways," *J. China Univ. Mining Technol.*, vol. 19, no. 2, pp. 30–37, 1989. [Online]. Available: https://kns.cnki.net/kcms/detail/detail.aspx?dbcode=CJFD&dbname=CJFD8589&filename=ZGKD198902005&v=jZdQKQv53VgAuoUTpbJqyXOYZgoREaC%25mmd2BWJcNd7Fhsxe3Tdz6JeopjFwI9DxsehpH

[32] H. Zhaofeng and C. Guohua, "High-stress soft rock roadway support technology," *Mine Pressure Roof Manage.*, no. 4, pp. 38–39, 2003, doi: 1003-5923(2003)04-0038-02.

[33] L. Yinlong, W. Lianguo, Z. Bei, and L. Yujie, "Study on the optimization of the timing of bolt and grouting support for soft rock roadways," *Rock Soil Mech.*, vol. 33, no. 5, pp. 1395–1401, 2012, doi: 10.16285/j.rsm.2012.05.023.

[34] W. Zhongwen, F. Jianqin, X. Caichu, B. Yuewei, and J. Lei, "Method for determining reasonable support timing of the secondary lining of tunnels considering the creep characteristics of surrounding rock," *Chin. J. Rock Mech. Eng.*, vol. 29, no. S1, pp. 3241–3246, 2010. [Online]. Available: http://kns.cnki.net/kcms/detail/detail.aspx?FileName=YSLX2010S1095&DbName=CJFQ2010

[35] N. Ze. *Improvement and Application of Evolutionary Structural Optimization Method*. Changsha University of Science and Technology. Accessed: 2013. [Online]. Available: https://kns.cnki.net/kcms/detail/detail.aspx?dbcode=CMFD&dbname=CMFD201402&filename=1013303112.nh&v=olDWONLsNgsUKZHpI7ggF4cPg4cDx3UEds1fj1m0BrOpbzv2SdY1dUrSBQ%25mmd2BYSp6J

[36] F. Wang, R. Liu, Q. Hu, and X. Chen, "Cascade convolutional neural network with progressive optimization for motor fault diagnosis under nonstationary conditions," *IEEE Trans. Ind. Informat.*, vol. 17, no. 4, pp. 2511–2521, Apr. 2021, doi: 10.1109/TII.2020.3003353.

YUE WU is currently pursuing the Ph.D. degree in geotechnical engineering with the Shandong University of Science and Technology, China. His research interests include deep rock fracture failure, grouting, support, and inoculation mechanism of discontinuous fractured rock.

WEIGUO QIAO received the Ph.D. degree. He is currently a Professor and a Ph.D. Supervisor of Geotechnical Engineering, a Famous Teaching Teacher with the Shandong University of Science and Technology, and the Director of the Academic Affairs Office. He is also a Vice Chairman of the Shandong Rock Mechanics and Engineering Society, the Executive Director of the Underground Engineering Branch, China Rock Mechanics and Engineering Society, a member of the Rock Mechanics and Support Professional Committee of China Coal Society, a Mine Construction Expert of the China Coal Industry Technical Committee, support of China Coal Industry Association Expert, won the title of Excellent Talents in China's Coal Industry Technology Innovation, Excellent Talents in the New Century from the Ministry of Education, and the Young and Middle-aged Experts with Outstanding Contributions in Shandong Province.

YANZHI LI is currently pursuing the Ph.D. degree in geotechnical engineering with the Shandong University of Science and Technology, China. His research interests include deep well sandstone microscopic pore seepage characteristics and cavity expansion grouting water plugging mechanism.

YABING JIAO received the master's degree from the Shandong University of Science and Technology, China. His research interests include deep underground engineering support and surrounding rock grouting water plugging.

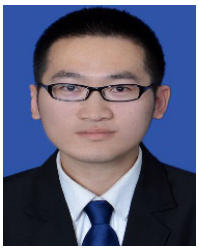

SHUAI ZHANG is currently pursuing the Ph.D. degree in geotechnical engineering with the Shandong University of Science and Technology, China. His research interests include grouting support for micro-fractured rock masses and seepage law of cement slurry.

ZONGHAO ZHANG received the master's degree from the Shandong University of Science and Technology, China. His research interest includes deep underground engineering support.

HUINI LIU is currently pursuing the master's degree in geotechnical engineering with the Shandong University of Science and Technology, China. His research interests include rock micropore seepage characteristics and grouting water plugging.